Inorg. Chem. **2006**, *45*, 7788–7798

Influence of Solvent and Weak C–H···O Contacts in the Self-Assembled $[Pt_2M_4\{C{\equiv}C(3\text{-}OMe)C_6H_4\}_8]$ (M = Cu, Ag) Clusters and Their Role in the Luminescence Behavior

Belén Gil,[†] Juan Forniés,[‡] Julio Gómez,[†] Elena Lalinde,*[,†] Antonio Martín,[‡] and M. Teresa Moreno[†]

Departamento de Química-Grupo de Síntesis Química de La Rioja, UA-CSIC, Universidad de La Rioja, 26006 Logroño, Spain, and Departamento de Química Inorgánica, Instituto de Ciencia de Materiales de Aragón, Universidad de Zaragoza−Consejo Superior de Investigaciones Científicas, 50009 Zaragoza, Spain

Received May 15, 2006

New alkynyl complexes $[Pt_2M_4\{C{\equiv}C(3\text{-}OMe)C_6H_4\}_8]$ (M = Ag **1**, Cu **2**) have been synthesized and their structures and properties compared to those of related $[Pt_2M_4(C{\equiv}CPh)_8]$ compounds. For the Pt–Ag derivatives, the X-ray structures of the discrete yellow solvate monomer, $[Pt_2Ag_4\{C{\equiv}C(3\text{-}OMe)C_6H_4\}_8]\cdot 2THF$ ([**1·2THF**]), and the dark garnet unsolvated polymeric form, $[Pt_2Ag_4\{C{\equiv}C(3\text{-}OMe)C_6H_4\}_8]_\infty$ ($[\mathbf{1}]_\infty$), are presented. The yellow form ([**1·2THF**]) exhibits a distorted octahedral geometry of the metal centers with the platinum atoms mutually trans and the four silver atoms in the equatorial plane. Pairs of Ag atoms are weakly bridged by THF molecules [μ-Ag$_2$···O(THF)]. The garnet form ($[\mathbf{1}]_\infty$) has an unprecedented infinite stacked chain of octahedral clusters linked by short Pt···Pt bonds (3.1458(8) Å). In both forms, different types of weak C–H···O (OMe) hydrogen bonds are observed. For comparative purposes, we have also provided the crystal structures of the yellow monomer form, $[Pt_2Ag_4(C{\equiv}CPh)_8]\cdot CHCl_3$, and the red dimer form, $[Pt_2Ag_4(C{\equiv}CPh)_8]_2$ (Pt–Pt 3.221(2) Å). These clusters display intense photoluminescence in both solution and the solid state, at room temperature and 77 K. The emission observed for the yellow form [**1·2THF**] in the solid state is assigned to a ^{3}MLM′CT [Pt(d)/π(C≡CR) → Pt(p$_z$)/Ag(sp)/π*(C≡CR)] state modified by Pt···Ag, Ag...Ag, and Ag···(THF) contacts. However, in the garnet form $[\mathbf{1}]_\infty$ and in **2**, the emissions are related to the axial Pt–Pt bonds and are assigned as phosphorescence from a metal–metal-to-ligand charge-transfer (^{3}MMLCT) excited state ($[\mathbf{1}]_\infty$), or an admixture of a metal–metal (Pt–Pt) centered ^{3}(dσ*p$_z\sigma$) and ^{3}MMLCT excited state (**2**). For **1**, a remarkable quenching and a shift to higher energies in the emission is observed on changing from CH_2Cl_2 to THF, and for both **1** and **2**, the emission spectra at 77 K varies with the concentration, showing their tendency to stack even in glass.

Introduction

The development of supramolecular systems based on weak noncovalent interactions is a topic of current research because of the unusual structural and spectroscopic properties of these systems.[1−15] In particular, the sensitivity of these systems' spectroscopic properties, such as absorption and luminescence, to environmental factors may be useful in sensing devices.[4,6,8−15] The tendency of square-planar plati-

* To whom correspondence should be addressed. E-mail: elena.lalinde@dq.unirioja.es.
[†] Universidad de La Rioja, UA-CSIC.
[‡] Universidad de Zaragoza−CSIC.

(1) Lehn, J. M. *Supramolecular Chemistry: Concepts and Perspectives*; VCH: Weinheim, Germany, 1995.
(2) Braga, D.; Grepioni, F. *Chem. Commun.* **2005**, 3635 and references therein.
(3) Yam, V. W. W. *J. Organomet. Chem.* **2004**, *689*, 1393.
(4) Yu, S. Y.; Zhang, Z. X.; Cheng, E. C. C.; Li, Y. Z.; Yam, V. W. W.; Huang, H. P.; Zhang, R. *J. Am. Chem. Soc.* **2005**, *127*, 17994.
(5) Roesky, H. W.; Adruh, M. *Coord. Chem. Rev.* **2003**, *236*, 91.
(6) Schuster, O.; Monkowins, U.; Schmidbaur, H.; Ray, R. S.; Krüger, S.; Rösch, N. *Organometallics* **2006**, *25*, 1004.
(7) Gale, P. A.; Light, M. E.; Quesada, R. *Chem. Commun.* **2005**, 5864.
(8) Omary, M. A.; Rawashdeh-Omary, M. A.; Gonser, M. W. A.; Elbjeirami, O.; Grimes, T.; Cundari, T. R.; Diyabalanage, H. V. K.; Gamage, C. S. P.; Dias, H. V. R. *Inorg. Chem.* **2005**, *44*, 8200.
(9) White-Morris, R. L.; Olmstead, M. M.; Attar, S.; Balch, A. L. *Inorg. Chem.* **2005**, *44*, 5021.
(10) Mohamed, A. A.; Rawashdeh-Omary, M. A.; Omary, M. A.; Fackler, J. P., Jr. *Dalton Trans.* **2005**, 2597 and references therein.
(11) Huang, X. C.; Zheng, S. L.; Zhang, J. P.; Chen, X. M. *Eur. J. Inorg. Chem.* **2004**, 1024.
(12) Haneline, M. R.; Tsunoda, M.; Gabbaï, F. P. *J. Am. Chem. Soc.* **2002**, *124*, 3737.

10.1021/ic0608344 CCC: $33.50 © 2006 American Chemical Society
Published on Web 08/22/2006

num(II) complexes to form stacking structures controlled by metal···metal and $\pi\cdots\pi$ ligand interactions, which leads to characteristic luminescence, is now well-established.[16−29] The more common structural types are linear chain structures with a constant Pt···Pt or $\pi\cdots\pi$ separation or dimer structures that exhibit emissions generally assigned as ^{3}MMLCT or that are excimeric $\pi\pi^*$ in nature.

Our group has long been interested in homo- and heteropolymetal alkynyl platinum complexes,[29−34] and one of our current research interests is the use of alkynyl platinate(II) substrates such as the homoleptic $[Pt(C{\equiv}CR)_4]^{2-}$ derivatives[35,36] as building blocks in molecule-based materials.[32,35,37−41] Diverse Pt−M with closed (M = Cu, Ag, Au, Cd)[35,42−47] or subclosed shell (Tl(I))[48,49] heteropolynuclear cluster complexes, which exhibit intriguing photophysical properties associated with metal−metal and η^2-bonding interactions, have been prepared. A similar synthetic strategy has been also employed by Yam et al.[50,51] and more recently by Chen et al.[52,53] to form luminescent heteropolynuclear platinum−copper or silver complexes.

Several years ago, we described the preparation of several Pt−group 11 alkynyl bridging complexes of stoichiometry $[Pt_2M_4(C{\equiv}CR)_8]$ (R = Ph, *t*-Bu; M = Cu, Ag, Au).[35] More recently, we reported, together with Yam et al., the rich polymorphism and interesting luminescence properties exhibited by the phenylethynyl derivatives.[43,50] We observed that for $[Pt_2Ag_4(C{\equiv}CPh)_8]$, yellow (monomer) and red (a dimer formed by two clusters linked by a Pt···Pt interaction of 3.221(2) Å) crystals are generated from concentrated $CHCl_3$/*n*-hexane solutions. For the related platinum−copper cluster, violet-green crystals, which were found to be formed by discrete trimers connected by two unsupported Pt···Pt interactions (2.995(1) Å),[43] and red crystals (dimers) with a longer Pt···Pt separation of 3.116(2) Å,[50] were obtained depending on the concentration. A third, yellow form easily separates upon treatment of the green and red solids with acetonitrile.[43] Considerable experimental work[30,32,48,49] and theoretical calculations[32] indicate that the metallophilic Pt(II)−Tl(I) interaction and the final structures and properties of alkynyl thallium−platinates can be fined-tuned by varying the ligands and substituents on the alkynyl ligands. In the same line, we now report the synthesis and luminescence behavior of $[Pt_2M_4${C≡C(3-OMe)C_6H_4}$_8]$ (M = Ag **1**, Cu **2**). X-ray structures are reported for a discrete yellow solvate monomer $[Pt_2Ag_4${C≡C(3-OMe)C_6H_4}$_8]$·2THF, [**1·2THF**], and an unprecedented dark violet polymer of $[Pt_2Ag_4$-{C≡C(3-OMe)C_6H_4}$_8]$, $[\mathbf{1}]_\infty$, which is formed by an infinite stacking of clusters linked by relatively short Pt···Pt bonds of 3.1458(8) Å. For the purpose of comparison, we have also included the crystal structures of $[Pt_2Ag_4(C{\equiv}CPh)_8]$·$CHCl_3$ and $[Pt_2Ag_4(C{\equiv}CPh)_8]_2$ (see the Supporting Information).

Experimental Section

General Considerations. All reactions and manipulations were carried out under a nitrogen atmosphere using Schlenk techniques and distilled solvents, purified by known procedures. IR spectra

(13) Lee, Y. A.; McGarrah, J. E.; Lachicotte, R. J.; Eisenberg, R. *J. Am. Chem. Soc.* **2002**, *124*, 10662.
(14) Olmstead, M. M.; Jiang, F.; Attar, S.; Balch, A. L. *J. Am. Chem. Soc.* **2001**, *123*, 3260.
(15) Mansour, M. A.; Connick, W. B.; Lachicotte, R. J.; Gysling, H. J.; Eisenberg, R. *J. Am. Chem. Soc.* **1998**, *120*, 1329.
(16) Novoa, J. J.; Aullón, G.; Alemany, P.; Alvarez, S. *J. Am. Chem. Soc.* **1995**, *117*, 7169.
(17) Buss, C. E.; Mann, K. R. *J. Am. Chem. Soc.* **2002**, *124*, 1031.
(18) Grove, L. J.; Rennekamp, J. M.; Jude, H.; Connick, W. B. *J. Am. Chem. Soc.* **2004**, *126*, 1594.
(19) Stoyanov, S. R.; Villegas, J. M.; Rillema, D. P. *Inorg. Chem.* **2003**, *42*, 7852 and references therein.
(20) Lu, W.; Chan, M. C. W.; Zhu, N.; Che, C. M.; Li, C.; Hui, Z. *J. Am. Chem. Soc.* **2004**, *126*, 7639.
(21) Wadov, T. J.; Wang, Q. M.; Kim, Y. J.; Flaschenreim, C.; Blanton, T. N.; Eisenbereg, R. *J. Am. Chem. Soc*. **2004**, *126*, 16841.
(22) Farley, S. J.; Rochester, D. L.; Thompson, A. L.; Howard, J. A. K.; Williams, J. A. G. *Inorg. Chem.* **2005**, *44*, 9690.
(23) Yam, V. W. W.; Tang, R. P. L.; Wong, K. M. C.; Lu, X. X.; Cheung, K. K.; Zhu, N. *Chem.—Eur. J.* **2002**, *8*, 4066.
(24) Yam, V. W. W.; Wong, K. M. C.; Zhu, N. *J. Am. Chem. Soc.* **2002**, *124*, 6506.
(25) Palmans, R.; MacQueen, D. B.; Pierpont, C. G.; Frank, A. J. *J. Am. Chem. Soc.* **1996**, *118*, 12647.
(26) Bailey, J. A.; Hill, M. G.; Marsh, R. E.; Miskowski, V. M.; Schaefer, W. P.; Gray, H. B. *Inorg. Chem.* **1995**, *34*, 4591.
(27) Büchner, R.; Cunningham, C. T.; Field, J. S.; Haines, R. J.; McMillin, D. R.; Summerton, G. C. *J. Chem. Soc., Dalton Trans.* **1999**, 711.
(28) Lai, S. W.; Chan, M. C. W.; Cheung, T. C.; Peng, S. M.; Che, C. M. *Inorg. Chem.* **1999**, *38*, 4046.
(29) Forniés, J.; Lalinde, E. *J. Chem. Soc., Dalton Trans.* **1996**, 2587.
(30) Ara, I.; Berenguer, J. R.; Forniés, J.; Gómez, J.; Lalinde, E.; Merino, R. I. *Inorg. Chem.* **1997**, *36*, 6461.
(31) Berenguer, J. R.; Eguizábal, E.; Falvello, L. R.; Forniés, J.; Lalinde, E.; Martín, A. *Organometallics* **2000**, *19*, 490.
(32) Charmant, J. P. H.; Forniés, J.; Gómez, J.; Lalinde, E.; Merino, R. I.; Moreno, M. T.; Orpen, A. G. *Organometallics* **2003**, *22*, 652.
(33) Ara, I.; Berenguer, J. R.; Eguizábal, E.; Forniés, J.; Gómez, J.; Lalinde, E. *J. Organomet. Chem.* **2003**, *670*, 221 and references therein.
(34) Forniés, J.; Ibañez, S.; Martín, A.; Gil, B.; Lalinde, E.; Moreno, M. T. *Organometallics* **2004**, *23*, 3963.
(35) Espinet, P.; Forniés, J.; Lalinde, E.; Martínez, F.; Moreno, M. T.; Ruiz, A.; Tomás, M.; Welch, A. J. *J. Chem. Soc., Dalton Trans.* **1990**, 791.
(36) Benito, J.; Berenguer, J. R.; Forniés, J.; Gil, B.; Gómez, J.; Lalinde, E. *Dalton Trans.* **2003**, 4331.
(37) Ara, I.; Berenguer, J. R.; Forniés, J.; Lalinde, E. *Organometallics* **1997**, *16*, 3921.
(38) Ara, I.; Berenguer, J. R.; Forniés, J.; Lalinde, E. *Inorg. Chim. Acta* **1997**, *264*, 199.
(39) Falvello, L. R.; Forniés, J.; Lalinde, E.; Martín, A.; Moreno, M. T.; Sacristán, J. *Chem. Commun.* **1998**, 141.
(40) Ara, I.; Berenguer, J. R.; Eguizábal, E.; Forniés, J.; Lalinde, E. *Organometallics* **2001**, *20*, 2686.
(41) Berenguer, J. R.; Forniés, J.; Lalinde, E.; Martínez, F. *Organometallics* **1996**, *15*, 4537.
(42) Ara, I.; Forniés, J.; Gómez, J.; Lalinde, E.; Merino, R. I.; Moreno, M. T. *Inorg. Chem. Commun.* **1999**, *2*, 62.
(43) Charmant, J. P. H.; Forniés, J.; Gómez, J.; Lalinde, E.; Merino, R. I.; Moreno, M. T.; Orpen, A. G. *Organometallics* **1999**, *18*, 3353.
(44) Charmant, J. P. H.; Falvello, L. R.; Forniés, J.; Gómez, J.; Lalinde, E.; Moreno, M. T.; Orpen, A. G.; Rueda, A. *Chem. Commun.* **1999**, 2045.
(45) Ara, I.; Forniés, J.; Gómez, J.; Lalinde, E.; Moreno, M. T. *Organometallics* **2000**, *19*, 3137.
(46) Forniés, J.; Gómez, J.; Lalinde, E.; Moreno, M. T. *Inorg. Chem.* **2001**, *40*, 5415.
(47) Fernández, J.; Forniés, J.; Gil, B.; Gómez, J.; Moreno, M. T.; Lalinde, E. *Organometallics* **2006**, *25*, 2274.
(48) Berenguer, J. R.; Forniés, J.; Gómez, J.; Lalinde, E.; Moreno, M. T. *Organometallics* **2001**, *20*, 4847.
(49) Berenguer, J. R.; Forniés, J.; Gil, B.; Lalinde, E. *Chem.—Eur. J.* **2006**, *12*, 785.
(50) Yam, V. W. W.; Yu, K. L.; Cheung, K. K. *J. Chem. Soc., Dalton Trans.* **1999**, 2913.
(51) Yam, V. W. W.; Hui, C. K.; Yu, S. Y.; Zhu, N. *Inorg. Chem.* **2004**, *43*, 812.
(52) Wei, Q. H.; Yin, G. Q.; Ma, Z.; Shi, L. X.; Chen, Z. N. *Chem. Commun.* **2003**, 2188.
(53) Yin, G. Q.; Wei, Q. H.; Zhang, L. Y.; Chen, Z. N. *Organometallics* **2006**, *25*, 580.

Table 1. Crystal Data and Structure Refinement Details for the Complexes

	[**1·2THF**]	$[\mathbf{1}]_\infty$	$[Pt_2Ag_4(C{\equiv}CPh)_8]\cdot CHCl_3$
empirical formula	$C_{80}H_{72}Ag_4O_{10}Pt_2$	$C_{144}H_{112}Ag_8O_{16}Pt_4$	$C_{65}H_{41}Ag_4Cl_3Pt_2$
fw	2015.04	3741.66	1749.99
T (K)	173(1)	173(1)	150(2)
wavelength (Å)	0.71073	0.71073	0.71073
cryst syst	triclinic	orthorhombic	triclinic
space group	$P\bar{1}$	*Pnaa*	$P\bar{1}$
a (Å)	10.7620(2)	14.87300(10)	11.6956(13)
b (Å)	14.6654(3)	16.7280(2)	15.1811(8)
c (Å)	23.8645(6)	24.5610(3)	16.858(2)
α (deg)	73.7330(10)	90	91.544(14)
β (deg)	77.5840(10)	90	108.992(14)
γ (deg)	78.9990(10)	90	91.305(11)
V (Å^3)	3496.73(13)	6110.67(11)	2827.6(5)
Z	2	2	2
d_{calcd} (mg/m^3)	1.914	2.034	2.055
abs corr (mm^{-1})	5.144	5.876	6.468
F(000)	1952	3584	1652
cryst size (mm^3)	0.10 × 0.10 × 0.10	0.30 × 0.05 × 0.05	0.40 × 0.30 × 0.30
2θ range (deg)	2.60−26.37	2.91−26.37	2.24−24.98
index ranges	$0 \le h \le 13$, $-17 \le k \le 18$, $-28 \le l \le 29$	$-18 \le h \le 18$, $-20 \le k \le 20$, $-30 \le l \le 30$	$0 \le h \le 13$, $-18 \le k \le 18$, $-19 \le l \le 18$
no. of reflns collected	14222	59872	10417
no. of independent reflns	14222 [R(int) = 0.0000]	6192 [R(int) = 0.0676]	9887 [R(int) = 0.0150]
data/restraints/params	14222/0/765	6192/0/225	9878/6/697
GOF on F^2 [a]	1.034	1.097	1.174
final R indices [$I > 2\sigma(I)$][a]	R1 = 0.0511, wR2 = 0.0938	R1 = 0.0710, wR2 = 0.1544	R1 = 0.0406, wR2 = 0.0871
R indices (all data)[a]	R1 = 0.0910, wR2 = 0.1084	R1 = 0.0947, wR2 = 0.1638	R1 = 0.0565, wR2 = 0.0970
largest diff. peak and hole (e Å^{-3})	1.562 and −1.709	2.108 and −1.804	2.069 and −2.013

[a] $R1 = \sum(|F_o| - |F_c|)/\sum|F_o|$; $wR2 = [\sum w(F_o^2 - F_c^2)^2/\sum wF_o^2]^{1/2}$; goodness of fit $= \{\sum[w(F_o^2 - F_c^2)^2]/(N_{obs} - N_{param})\}^{1/2}$; $w = [\sigma^2(F_o^2) + (g_1P)^2 + g_2P]^{-1}$; $P = [\max(F_o^2;0) + 2F_c^2]/3$.

were recorded on a Perkin−Elmer FT-IR 1000 and on a Nicolet Nexus FT-IR Spectrometer as Nujol mulls between polyethylene sheets. NMR spectra were recorded on Bruker ARX 300 and Bruker AVANCE 400 spectrometers and chemical shifts are reported in parts per million relative to external TMS (^{1}H, ^{13}C) or Na_2PtCl_6 in D_2O (^{195}Pt). Elemental analyses were carried out with a Perkin-Elmer 2400 CHNS/O microanalyzer, and mass spectra were recorded on a Microflex MALDI-TOF Bruker spectrometer operating in the linear and reflector modes using dithranol as matrix. UV−visible spectra were obtained on a Hewlet Packard 8453 spectrometer. Emission and excitation spectra were obtained on a Jobin-Yvon Horiba Fluorolog 3−11 Tau-3 spectrofluorimeter, with lifetimes measured operating in the phosphorimeter mode or in the phase-modulation mode. Phase shift and modulation were recorded over the frequency range of 0.1−10 MHz and data were fitted using the Jobin- Yvon software package. The precursor $(NBu_4)_2[Pt\{C{\equiv}C(3\text{-}OMe)C_6H_4\}_4]$ was prepared as previously described.[36]

Synthesis of $[Pt_2Ag_4\{C{\equiv}C(3\text{-}OMe)C_6H_4\}_8]$ (1). $AgClO_4$ (34 mg, 0.166 mmol) was added to a solution of $(NBu_4)_2[Pt\{C{\equiv}C(3\text{-}OMe)C_6H_4\}_4]$ (100 mg, 0.084 mmol) in acetone (10 mL), and a yellow solid immediately began to precipitate. After 30 min of the solution being stirred, the solid was filtered off, washed with cold acetone, and air-dried (52 mg, 56%). Anal. Calcd for $C_{72}H_{56}Ag_4Pt_2O_8$ (1870.90): C, 46.22; H, 3.02. Found C, 45.86; H, 2.98. MALDI-TOF (+): *m*/*z* 1978 $[M + Ag]^+$ 8%; 1872 $[M]^+$ 10%; 1739 $[M\text{-}\{C{\equiv}C(3\text{-}OMe)C_6H_4\}]^+$ 14%. IR (cm^{-1}) yellow form: $\tilde{\nu}$(C≡C) 2033s. ^{1}H NMR ($CDCl_3$, 300.13 MHz, 298 K, δ): 7.05−6.90 (m, $H^{2,4,5}$, 24H, C_6H_4); 6.79 (d, J = 7.3 Hz, H^6, 8H, C_6H_4); 3.66 (s, 24H, $-OCH_3$). $^{13}C\{^1H\}$ NMR ($CDCl_3$, 100.62 MHz, 298 K, δ): 159.7 (s, C^3); 129.5, 125.8 (s, $C^{2,4}$); 125.1 (s, C^1); 117.5, 115.5 (s, $C^{5,6}$) [(3-OMe)C_6H_4]; 113.8 [s, ^2J(C−Pt) = 295.8 Hz, ≡C_β]; 79.2 [s, ^1J(C−Pt) = 908.1 Hz, C_α≡]; 55.6 [s, OMe, (3-OMe)C_6H_4]. ^{195}Pt ($CDCl_3$, 86.02 MHz, 298 K, δ): −3792.8 [q, $^1J(^{195}Pt\text{-}^{107,109}Ag) \approx 85$ Hz].

Synthesis of [1·2THF]. A similar reaction carried out in THF, starting from $(NBu_4)_2[Pt\{C{\equiv}C(3\text{-}OMe)C_6H_4\}_4]$ (100 mg, 0.084 mmol) and $AgClO_4$ (34 mg, 0.166 mmol), generates [**1·2THF**] as a yellow microcrystalline solid (54 mg, 58%). Anal. Calcd for $C_{80}H_{72}Ag_4Pt_2O_{10}$ (2010.06): C, 47.68; H, 3.60. Found C, 47.41; H, 3.82. IR (cm^{-1}): $\tilde{\nu}$(C≡C) 2039s.

Crystals of $[\mathbf{1}]_\infty$. Garnet crystals of $[\mathbf{1}]_\infty$ were grown by slow diffusion of *n*-hexane into a concentrated CH_2Cl_2 solution of **1** at room temperature. IR (cm^{-1}): $\tilde{\nu}$(C≡C) 2029s.

Synthesis of $[Pt_2Cu_4\{C{\equiv}C(3\text{-}OMe)C_6H_4\}_4]_\infty$ (2). $(NBu_4)_2[Pt\{C{\equiv}C(3\text{-}OMe)C_6H_4\}_4]$ (150 mg, 0.124 mmol) was added to a suspension of CuCl (25 mg, 0.249 mmol) and $NaClO_4$ (46 mg, 0.374 mmol) in acetone (20 mL). The mixture was stirred for 2 h at room temperature, and the solvent was then evaporated in vacuo. The addition of cold EtOH gave a very dark garnet precipitate, which was filtered off, washed successively with cold EtOH and cold acetone, and air-dried (89 mg, 85%). Anal. Calcd for $C_{72}H_{56}Cu_4Pt_2O_8\cdot 3/4\ CH_2Cl_2$ (1757.29): C, 48.48; H, 3.27. Found C, 48.06; H, 3.01. MALDI-TOF(+): *m*/*z* 1757 $[M + Cu]^+$ 33%. IR (cm^{-1}): $\tilde{\nu}$(C≡C) 2014s. ^{1}H NMR ($CDCl_3$, 300.13 MHz, 298 K, δ): 7.01−6.91 (m, $H^{4,5}$, 16H, C_6H_4); 6.85 (s, H^2, 8H, C_6H_4); 6.74 (d, J = 7.3 Hz, H^6, 8H, C_6H_4); 3.50 (s, 24H, $-OCH_3$). $^{13}C\{^1H\}$ NMR (CD_2Cl_2, 100.62 MHz, 298 K, δ): 159.4 (s, C^3); 129.2 (s, $C^{2,4}$); 125.2 (s, C^1); 124.6 (s, $C^{2,4}$); 116.5, 115.3 (s, $C^{5,6}$) [(3-OMe)C_6H_4]; 112.6 [s, ^2J(C−Pt) = 288.3 Hz, ≡C_β]; 86.4 [s, ^1J(C−Pt) = 933.9 Hz, C_α≡]; 55.0 [s, OMe, (3-OMe)C_6H_4]. ^{195}Pt (CD_2Cl_2, 86.02 MHz, 298 K, δ): −4119.4 (s).

$[Pt_2Ag_4(C{\equiv}CPh)_8]$.[35] $^{13}C\{^1H\}$ NMR (CD_2Cl_2, 100.62 MHz, 298 K, δ): 132.5 (s, C^2); 128.3 (s, C^3); 128.2 (s, C^4); 123.7 [s, ^3J(Pt−C) = 18.2 Hz, C^1] (Ph); 113.1 [s, ^2J(C−Pt) = 298.1 Hz, ≡C_β]; 79.3 [s, ^1J(C−Pt) = 900.3 Hz, C_α≡]. ^{195}Pt (CD_2Cl_2, 86.02 MHz, 298 K, δ): −3793.9 (s, vbr).

X-ray Crystallography. Table 1 reports details of the structural analyses for complexes [**1·2THF**], $[\mathbf{1}]_\infty$, and $[Pt_2Ag_4(C{\equiv}CPh)_8]\cdot CHCl_3$. For complex $[Pt_2Ag_4(C{\equiv}CPh)_8]_2$, deep red crystals were

grown by slow diffusion of hexane into a CH_2Cl_2 solution at room temperature. Unfortunately, the poor quality of all crystals studied precluded a good characterization by X-ray diffraction and only the connectivity is given (see the Supporting Information, Figure S1). Deep red crystals of [**1**]$_\infty$ and yellow crystals of [Pt_2Ag_4-(C≡CPh)$_8$]·$CHCl_3$ were obtained by slow diffusion of hexane into a dichloromethane or chloroform solution, respectively, at room temperature, whereas yellow crystals of [**1·2THF**] were obtained by allowing a tetrahydrofuran solution of this complex to evaporate at room temperature. Complexes [**1·2THF**] and [Pt_2Ag_4(C≡CPh)$_8$]·$CHCl_3$ crystallize, each with two independent but very similar half molecules per asymmetric unit and a molecule of THF and chloroform, respectively. For complexes [**1·2THF**] and [**1**]$_\infty$, X-ray intensity data were collected with a NONIUS κCCD area-detector diffractometer, and for [Pt_2Ag_4(C≡CPh)$_8$]·$CHCl_3$, with a Enraf-Nonius CAD4 diffractometer using graphite-monochromated Mo−K$_\alpha$ *X*-radiation. Images were processed using the DENZO and SCALEPACK suite of programs,[54] carrying out the absorption correction at this point for complex [**1·2THF**]. For complex [**1**]$_\infty$, the absorption correction was performed using SORTAV,[55] and for [Pt_2Ag_4(C≡CPh)$_8$]·$CHCl_3$, it was applied based on 720 azimuthal scan data[56] (maximum and minimum transmission coefficients were 0.933 and 0.697). The structures were solved by direct methods using the SHELXL-97 program[57] for complexes [**1·2THF**] and [**1**]$_\infty$, and by Patterson using the SHELXL-93[58] program for complex [Pt_2Ag_4(C≡CPh)$_8$]·$CHCl_3$; structures were refined by full-matrix least squares on F^2 with SHELXL-97 or SHELXL-93. All non-hydrogen atoms were assigned anisotropic displacement parameters. The hydrogen atoms were constrained to idealized geometries, fixing isotropic displacement parameters of 1.2 times the U_{iso} value of their attached carbons for phenyl and methylene hydrogens and 1.5 for the methyl groups. For [Pt_2Ag_4(C≡CPh)$_8$]·$CHCl_3$, the carbon atom of the chloroform solvent molecule lies an inversion center and thus the chlorine atoms show a disorder over two positions (0.5/0.5 occupancy) related by this inversion center. For the disordered chloroform, the C−Cl distances were constrained to idealized geometries. For complexes [**1**]$_\infty$ and [Pt_2Ag_4(C≡CPh)$_8$]·$CHCl_3$, residual peaks bigger than 1 e Å^{-3} have been observed in the final map but are located very close to some metal atom and have no chemical meaning. For complexes [**1·2THF**] and [**1**]$_\infty$, common sets of thermal anisotropic parameters were used for some atoms.

Results and Discussion

Synthesis and Characterization. Compound [Pt_2Ag_4-{C≡C(3-OMe)C$_6$H$_4$}$_8$] (**1**) was obtained as a yellow solid by reaction of $(NBu_4)_2$[Pt{C≡C(3-OMe)C$_6$H$_4$}$_4$] with $AgClO_4$. Subsequent recrystallization from THF or, alternatively, carrying out the reaction in THF solution, afforded the adduct **[1·2THF]** as a yellow microcrystalline solid, as confirmed by analytical and X-ray crystallographic data. Slow diffusion of *n*-hexane into a dichloromethane solution of **1** gave garnet crystals identified as an infinite chain of clusters, [**1**]$_\infty$, connected by axial Pt···Pt interactions (3.1458-(8) Å). The related platinum−copper derivative **2** was prepared as a very dark garnet (nearly black) solid by treating $(NBu_4)_2$[Pt{C≡C(3-OMe)C$_6$H$_4$}$_4$] with CuCl in the presence of an excess of $NaClO_4$ in acetone. **2** is only soluble in chlorinated solvents such as CH_2Cl_2 or $CHCl_3$. All attempts to obtain crystals of **2** suitable for X-ray diffraction were unsuccessful, but its color and optical properties (luminescence) suggest it forms an infinite chain of hexanuclear clusters [Pt_2Cu_4{C≡C(3-OMe)C$_6$H$_4$}$_8$]$_\infty$ similar to that of [**1**]$_\infty$.

Yellow monomer **1** shows $\tilde{\nu}$(C≡C) stretching at 2033 cm^{-1}, shifted to lower frequency in relation to that of the homoleptic precursor (2078 cm^{-1}), consistent with coordination of silver centers to the alkyne unit. Interestingly, in the adduct [**1·2THF**], this band occurs at 2039 cm^{-1}, suggesting a weaker η^2-alkynyl bonding as a consequence of the Ag···(μ-THF) contacts, whereas in garnet form [**1**]$_\infty$, the band is slightly shifted to lower frequencies (2029 cm^{-1}). The related platinum−copper clusters show $\tilde{\nu}$(C≡C) at 2014 cm^{-1}, pointing to a stronger Cu-η^2(alkyne) bonding interaction. The MALDI-TOF(+) spectra of both clusters reveal the presence of heptanuclear [Pt_2M_5(C≡CR)$_8$]$^+$ cationic entities (*m*/*z* 1978, **1**; 1757, **2**) in the gas phase. The ^{13}C NMR spectra reveal that upon η^2-coordination to the d^{10} metal ions, the C$_\alpha$ and C$_\beta$ signals of precursor [Pt{C≡C(3-OMe)-C$_6$H$_4$}$_4$]$^{2-}$ (δ 119.4, J(Pt−C$_\alpha$) = 990.2; 102.6, ^2J(Pt−C$_\beta$) = 286 Hz, d^6 acetone) shift upfield for C$_\alpha$ (79.2, **1**; 86.4, **2**) and downfield for C$_\beta$ (δ 113.8, **1**; 112.6, **2**). Only coupling to ^{195}Pt is observed, the ^1J(Pt−C$_\alpha$) coupling being notably smaller in both clusters (J(Pt−C$_\alpha$) 908.1 Hz, **1**; 933.9 Hz, **2**) than in the precursor. For the purpose of comparison, we have also recorded the ^{13}C{^{1}H} NMR spectrum of [Pt_2Ag_4-(C≡CPh)$_8$]. The values of $\Delta\delta$ for both acetylenic carbons and the variation in ΔJ(Pt−C) are comparable to those seen in **1** (δC/J(Pt−C)(Hz) 79.3/900.3 (C$_\alpha$); 113.1/298.1 (C$_\beta$) in [Pt_2Ag_4(C≡CPh)$_8$] vs 120.9/989.8 (C$_\alpha$); 104.1/287.4 (C$_\beta$) in [Pt(C≡CPh)$_4$]$^{2-}$). The most remarkable difference is observed in the ^{195}Pt NMR spectra. Thus, whereas [Pt_2Ag_4-(C≡CPh)$_8$] exhibits a broad singlet centered at −3793.9 ppm, the signal is seen as a quintuplet in cluster **1** (see Figure 1) because of coupling to the four active ^{107,109}Ag nuclei (J(^{195}Pt−^{107,109}Ag) ≈ 85 Hz). In both **1** (δ −3792.8) and **2** (δ −4119.4), the platinum resonance is slightly shifted downfield in relation to the anionic precursor $(NBu_4)_2$[Pt-{C≡C(3-OMe)C$_6$H$_4$}$_4$] (δ −4167, $CDCl_3$, 298 K).

Crystal Structures. Crystals of [**1·2THF**] were grown by slow evaporation of a THF solution of **1** and crystals of [**1**]$_\infty$ were obtained by slow diffusion of *n*-hexane into a CH_2Cl_2 solution of **1**. Diffusion of *n*-hexane into a concentrated solution of [Pt_2Ag_4(C≡CPh)$_8$][35,43] in $CHCl_3$ or CH_2Cl_2 simultaneously forms yellow and red crystals. The X-ray crystallographic study of a yellow crystal obtained from $CHCl_3$ confirms the presence of one $CHCl_3$ molecule per cluster interacting with one of the platinum centers (Figure 2, Table 2). Despite many attempts, the crystal data of the red form of [Pt_2Ag_4(C≡CPh)$_8$]$_2$ were not good enough for a complete X-ray study. The best results were obtained from a red crystal obtained in CH_2Cl_2/*n*-hexane and at least

(54) Otwinowski, Z.; Minor, W. In *Methods in Enzymology*; Carter, C. V., Jr., Sweet, R. M., Eds.; Academic Press: New York, 1997; Vol. 276A, p 307.
(55) Blessing, R. H. *Acta Crystallogr., Sect. A* **1995**, *51*, 33.
(56) North, A. C. T.; Phillips, D. C.; Mathews, F. S. *Acta Crystallogr., Sect. A* **1968**, *24*, 351.
(57) Sheldrick, G. M. *SHELXL97, a Program for the Refinement of Crystal Structures*; University of Göttingen: Göttingen, Germany, 1997.
(58) Sheldrick, G. M. *A Program for Crystal Structure Determination.* University of Göttingen: Göttingen, Germany, 1993.

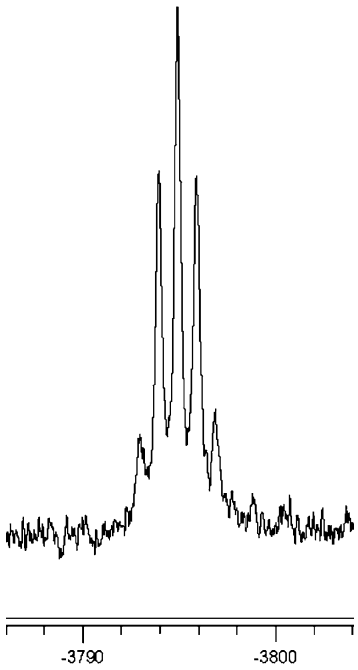

Figure 1. $^{195}Pt\{^{1}H\}$ NMR spectra of $[Pt_2Ag_4\{C{\equiv}C(3\text{-}OMe)C_6H_4\}_8]$ **1** in CD_3COCD_3 at 298 K

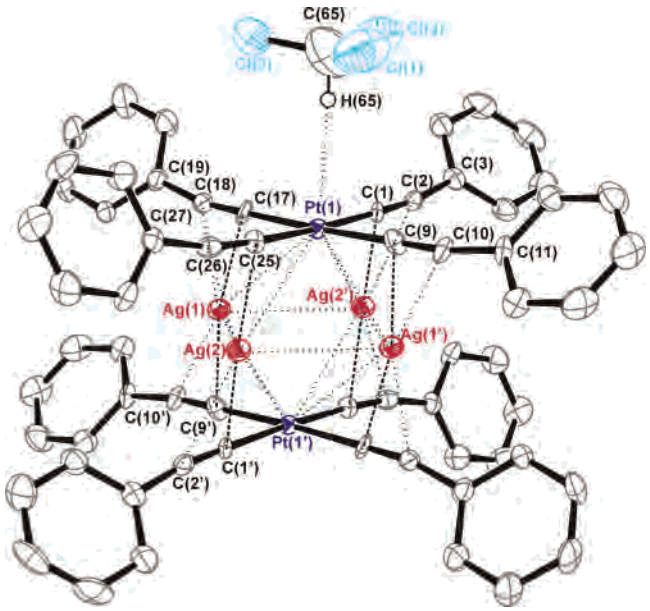

Figure 2. ORTEP view of $[Pt_2Ag_4(C{\equiv}CPh)_8]{\cdot}HCCl_3$ (molecule A) with 50% thermal contours, showing the interaction with the $CHCl_3$ molecule.

enables us to confirm that only two clusters are linked by a Pt···Pt contact of 3.221(2) Å (see the Supporting Information, Figure S1). Two crystallographically independent molecules A and B but with similar structural details were found in the unit cell of [**1·2THF**] and also in that of the yellow form of $[Pt_2Ag_4(C{\equiv}CPh)_8]{\cdot}CHCl_3$. An ORTEP drawing of the structure of molecule A of [**1·2THF**] is shown in Figure 3. Selected bonding parameters together with those of $[Pt_2Ag_4(C{\equiv}CPh)_8]{\cdot}CHCl_3$ (molecule A) and of $[\mathbf{1}]_\infty$ are listed in Table 2. Data and figures for molecules B are given in the Supporting Information (see the Supporting Information, Table S1, Figures S2 and S3).

The term employed in the literature to define two forms of a compound, the unsolvated and solvated forms with different crystal structures, is still a topic of debate. In many occasions, such systems have been considered "pseudopolymorphs"[59−61] because of the fact that they are different chemical entities and, therefore, are not real polymorphs. However, Seddon and others[62] argue that a compound and its solvate must necessarily have different crystal structures and they are not chemically identical. They prefer using the term solvate and not polymorph or pseudopolymorph.

The basic skeletons of the yellow form of [**1·2THF**] and $[Pt_2Ag_4(C{\equiv}CPh)_8]{\cdot}CHCl_3$ are similar. Both exhibit a distorted octahedral geometry of the metal centers with the platinum atoms in a mutually trans disposition and the four silver atoms in the equatorial plane. The two square-planar $Pt(C{\equiv}CR)_4$ fragments are found to be almost eclipsed with torsional angles $C_\alpha{-}Pt{-}Pt{-}C_\alpha'$ of 0.6° in [**1·2THF**] and 0.5° in $[Pt_2Ag_4(C{\equiv}CPh)_8]{\cdot}CHCl_3$. In [**1·2THF**], two molecules of tetrahydrofuran are weakly contacting with the silver centers in a μ-$(OC_4H_8)Ag_2$ bridging fashion with Ag(1)′−O(10) and Ag(2)−O(10) distances of 2.816 and 2.764 Å, respectively. These values compare to the Ag···O distances found in $[Ag_2(HPB)(ClO_4)_2(THF)_2]$[63] (HPB = hexaphenylbenzene) and (η^2-benzene)(η^1-benzene)-Ag_3-[1-H−CB_9Br_9]$_2$[NO_3](THF).[64] By contrast, the acidic proton of the $HCCl_3$ molecule in $[Pt_2Ag_4(C{\equiv}CPh)_8]{\cdot}CHCl_3$ is directed toward the basic platinum center ($\theta_{Pt\cdots H-C}$ = 168.43°) with a Pt···H separation of 2.719 Å. This distance is similar to that seen in $[Pt_2Tl_4(C{\equiv}Ct\text{-}Bu)_8]{\cdot}CHCl_3$[48] (2.725 Å) and in the range in which these types of M···H interactions have been reported in the literature.[65−69] Two short (2.9652(9) and 3.0162(9) Å) and two long (3.2323(9) and 3.2833(9) Å) Pt−Ag distances are found in $[Pt_2Ag_4(C{\equiv}CPh)_8]{\cdot}CHCl_3$. In [**1·2THF**], the corresponding distances are all similar (3.0268(7)−3.1864(7) Å) and shorter than the sum of van der Waals radii (3.45 Å), demonstrating, in accordance with the $^{195}Pt\{^{1}H\}$ NMR spectrum of **1**, the presence of Pt···Ag bonding interactions. The presence of μ(THF) contacting molecules as a bridging ligand between silver centers causes a remarkable difference between the Ag···Ag separations in [**1·2THF**] (3.0304(9) vs 3.2563(9) Å). In the phenylethynyl derivative, however, the Ag···Ag separations (3.1686(11) and 3.2319(10) Å) are identical within experimental error. The silver alkynyl π bonds are asymmetric with $Ag{-}C_\alpha$ distances shorter than $Ag{-}C_\beta$ bonds (Δ 0.127−0.387 Å) and comparable to those

(59) Desiraju, G. R. *Cryst. Growth Des.* **2004**, *4*, 1089.
(60) Mondal, R.; Howard, J. A. K.; Banerjee, R.; Desiraju, G. R. *Chem. Commun.* **2004**, 644.
(61) Nangia, A. *Cryst. Growth Des.* **2006**, *6*, 2.
(62) Seddon, K. R. *Cryst. Growth Des.* **2004**, *4*, 1087.
(63) Ning, G. L.; Munakata, M.; Wu, L. P.; Mekawa, M.; Suenaga, Y.; Kuroda-Sowa, T.; Sugimoto, K. *Inorg. Chem.* **1999**, *38*, 5668.
(64) Tsang, C. W.; Yang, Q.; Sze, E. T. P.; Mak, T. C. W.; Chan, D. T. W.; Xie, Z. *Inorg. Chem.* **2000**, *39*, 3582.
(65) Canty, A. J.; van Koten, G. *Acc. Chem. Res.* **1995**, *28*, 406.
(66) Casas, J. M.; Forniés, J.; Martín, A. *J. Chem. Soc., Dalton Trans.* **1997**, 1559 and references therein.
(67) Martín, A. *J. Chem. Educ.* **1999**, *76*, 578.
(68) Casas, J. M.; Diosdado, B. E.; Falvello, L. R.; Forniés, J.; Martín, A. *Inorg. Chem.* **2005**, *44*, 9444.
(69) Brammer, L. *Dalton Trans.* **2003**, 3145.

Table 2. Selected Bond Lengths (Å) and Angles (deg) for Complexes $[Pt_2Ag_4\{C{\equiv}C(3\text{-}OMe)C_6H_4\}_8]\cdot 2THF$ [**1·2THF**] (molecule A), $[Pt_2Ag_4\{C{\equiv}C(3\text{-}OMe)C_6H_4\}_8]_\infty$ [**1**]$_\infty$, and $[Pt_2Ag_4(C{\equiv}CPh)_8]\cdot CHCl_3$ **2·CHCl₃** (molecule A)

	[**1·2THF**][a] (molecule A)		[**1**]$_\infty$[b]		**[Pt₂Ag₄(C≡CPh)₈]·CHCl₃**[c] (molecule A)	
Ag−C_α	Ag(1)−C(10)	2.231(8)	Ag(1)−C(1)	2.205(11)	Ag(1)−C(9′)	2.209(10)
	Ag(1)−C(19′)	2.259(7)	Ag(1)−C(19′)	2.210(11)	Ag(1)−C(17)	2.226(10)
	Ag(2)−C(1)	2.258(8)	Ag(2)−C(10)	2.220(12)	Ag(2)−C(1′)	2.210(9)
	Ag(2)−C(28′)	2.249(8)	Ag(2)−C(28′)	2.215(11)	Ag(2)−C(25)	2.248(9)
Ag−C_β	Ag(1)−C(11)	2.479(8)	Ag(1)−C(2)	2.410(12)	Ag(1)−C(10′)	2.496(9)
	Ag(1)−C(20′)	2.426(8)	Ag(1)−C(20′)	2.404(12)	Ag(1) − C(18)	2.365(9)
	Ag(2)−C(2)	2.502(8)	Ag(2)−C(11)	2.391(12)	Ag(2)−C(2′)	2.597(9)
	Ag(2)−C(29′)	2.440(9)	Ag(2)−C(29′)	2.418(14)	Ag(2)−C(26)	2.375(9)
C_α−C_β	C(1)−C(2)	1.215(11)	C(1)−C(2)	1.227(19)	C(1)−C(2)	1.221(13)
	C(10)−C(11)	1.216(10)	C(10)−C(11)	1.197(19)	C(9)−C(10)	1.198(13)
	C(19)−C(20)	1.202(11)	C(19)−C(20)	1.211(18)	C(17)−C(18)	1.200(13)
	C(28)−C(29)	1.227(11)	C(28)−C(29)	1.23(2)	C(25)−C(26)	1.230(12)
Ag−Ag	Ag(1)−Ag(2)	3.2563(9)	Ag(1)−Ag(2)	3.2657(16)	Ag(1)−Ag(2)	3.2319(10)
	Ag(1)−(2′)	3.0304(9)	Ag(1)−Ag(2′)	3.2580(13)	Ag(1)−Ag(2′)	3.1686(11)
Pt−Ag	Pt(1)−Ag(1)	3.1631(7)	Pt(1)−Ag(1)	3.1346(10)	Pt(1)−Ag(1)	3.2323(9)
	Pt(1)−Ag(2)	3.0268(7)	Pt(1)−Ag(2)	3.1544(11)	Pt(1)−Ag(2)	3.2833(9)
	Pt(1)−Ag(1′)	3.1444(7)	Pt(2)−Ag(1′)	3.1539(10)	Pt(1)−Ag(1′)	3.0162(9)
	Pt(1)−Ag(2′)	3.1864(7)	Pt(2)−Ag(2′)	3.1570(11)	Pt(1)−Ag(2′)	2.9652(9)
Pt−Pt	Pt(1)−Pt(1′)	4.407	Pt(1)−Pt(2)	3.1458(8)	Pt(1)−Pt(1′)	4.317
			Pt(2)−Pt(1′)	4.291		
Pt−C_α−C_β	Pt(1) − C(1) −C(2)	174.6(8)	Pt(1)−C(1)−C(2)	176.6(13)	Pt(1)−C(1)−C(2)	176.4(8)
	Pt(1) − C(10) − C(11)	175.7(7)	Pt(1)−C(10)−C(11)	179.1(14)	Pt(1)−C(9)−C(10)	179.8(8)
	Pt(1)−C(19)−C(20)	175.8(7)	Pt(2)−C(19)−C(20)	178.3(14)	Pt(1)−C(17)−C(18)	179.1(8)
	Pt(1)−C(28)−C(29)	178.4(7)	Pt(2)−C(28)−C(29)	178.7(13)	Pt(1)−C(25)−C(26)	173.7(8)
C_α−C_β−C_γ	C(1)−C(2)−C(3)	173.2(9)	C(1)−C(2)−C(3)	163.2(13)	C(1)−C(2)−C(3)	171.8(10)
	C(10)−C(11)−C(12)	169.8(9)	C(10)−C(11)−C(12)	164.3(15)	C(9)−C(10)−C(11)	172.0(10)
	C(19)−C(20)−C(21)	171.0(9)	C(19)−C(20)−C(21)	164.4(15)	C(17)−C(18)−C(19)	168.7(10)
	C(28)−C(29)−C(30)	172.9(9)	C(28)−C(29)−C(30)	165.6(18)	C(25)−C(26)−C(27)	168.9(10)

[a] Symmetry transformations used to generate equivalent atoms: $-x+1, -y+1, -z+1$; $-x+2, -y+1, -z+2$. [b] Symmetry transformations used to generate equivalent atoms: $x, -y+{}^1/_2, -z+{}^1/_2$; $x+{}^1/_2, -y+{}^1/_2, z$; $x+{}^1/_2, y, -z+{}^1/_2$; $x-{}^1/_2, y, -z+{}^1/_2$. [c] Symmetry transformations used to generate equivalent atoms: $-x, -y+2, -z-2$; $-x+1, y+3, -z-1$.

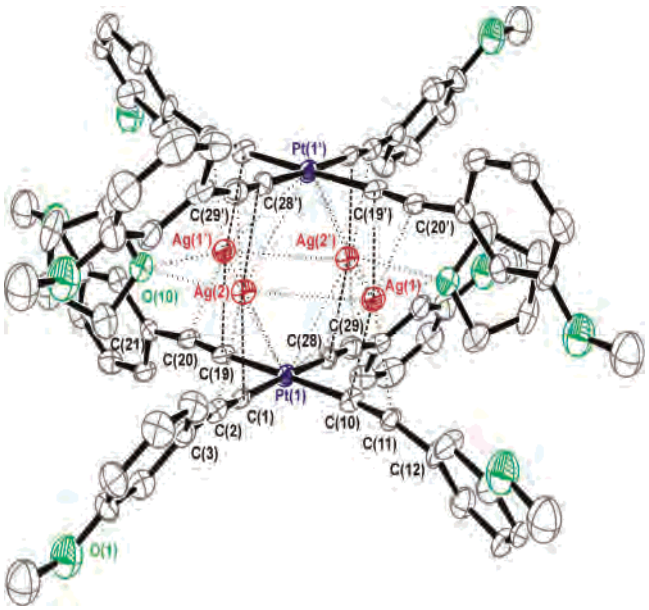

Figure 3. ORTEP view of $[Pt_2Ag_4\{C{\equiv}C(3\text{-}OMe)C_6H_4\}_8]\cdot 2THF$ [**1·2THF**] (molecule A) with 50% thermal contours.

found in related Ag(I)−π bond alkynyl bridging complexes.[29,40,42,45,51−53] The remaining structural details are unexceptional. However, in *m*-methoxyphenylalkynyl derivative [**1·2THF**], three different types of weak C−H···O(OMe) (d_{HO} = 2.363(6)−2.667(7) Å; θ_{C-H-O} = 132.72(7)−179.16(6)°) hydrogen bonds are observed in the extended lattice. As seen in Figure S4 (see the Supporting Information), the hydrogen bonds connect type A cluster molecules, affording chains of rectangular assemblies, and also molecules A with molecules B, giving rise to a final 3-D network.

The garnet form of $[Pt_2Ag_4\{C{\equiv}C(3\text{-}OMe)C_6H_4\}_8]$, [**1**]$_\infty$, crystallizes in orthorhombic needles of space group *Pnaa* with two formula units in the unit cell. The structure consists of a stacked chain of hexanuclear clusters linked by short Pt(1)−Pt(2) interactions (3.1458(8) Å) (Figure 4a) running parallel to the *a* axis of the unit cell (Figure 4b). As far as we know, this is the first example of a supramolecular array in which cluster units are connected only by Pt−Pt bonds. The Pt−Pt distance is slightly longer than that reported in the trimer derivative $[Pt_2Cu_4(C{\equiv}CPh)_8]_3$[43] and comparable to that seen in the corresponding dimer $[Pt_2Cu_4(C{\equiv}CPh)_8]_2$[50] (3.116(2) Å) and in the low range of Pt···Pt contacts previously found in crystal structures of dimers and chains (d < 3.5 Å).[70] As can be seen in the projection given in Figure 4c, the platinum atoms are superimposed, giving a nearly perfect linear chain. It is noteworthy that the individual clusters are rotated with respect to their neighbors, with a torsional angle C(1)−Pt(1)−Pt(2)−C(19) of 43.8(5)°, resulting in optimal stacking interactions by decreasing the steric repulsions of the *m*-methoxyphenyl substituents. It should be noted that within the cluster, the $Pt\{C{\equiv}C(3\text{-}OMe)C_6H_4\}_4$ units are also staggered with a smaller torsional angle C(1)−Pt(1)−Pt′(2)−C′(19) of 19.6°. This structural disposition contrasts with the orientation of the clusters found in the trimer $[Pt_2Cu_4(C{\equiv}CPh)_8]_3$, in which two eclipsed external

(70) Poater, A.; Moradell, S.; Pinilla, E.; Poater, J.; Sola, M.; Martínez, M. A.; LLobet, A. *Dalton Trans.* **2006**, 1188 and references given therein.

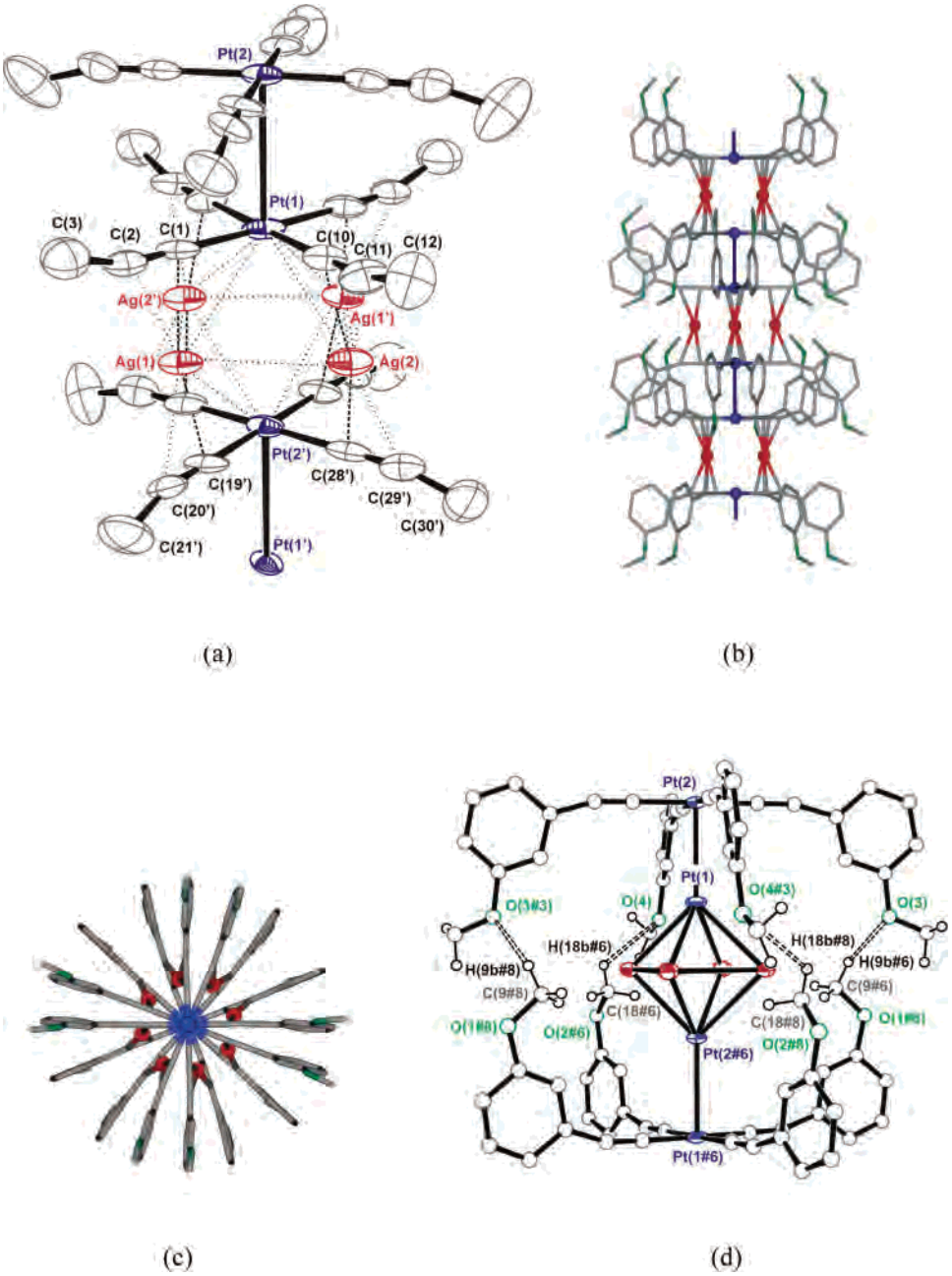

Figure 4. Molecular structure of $[Pt_2Ag_4\{C{\equiv}C(3\text{-}OMe)C_6H_4\}_8]_\infty$ [**1**]$_\infty$. (a) ORTEP view of molecule A, with 50% thermal contours. (b) Schematic view of three units of the chain. (c) Perspective view of the chain along the *a* axis. (d) Part of the chain showing the hydrogen bonds (dashed lines).

clusters are connected to a central staggered one (38°), suggesting a remarkable flexibility of the tetraalkynylplatinate(II) entities. In this trimer, $[Pt_2Cu_4(C{\equiv}CPh)_8]_3$, the resulting Pt_2Cu_4 octahedra are also successively twisted by 44°.

Interestingly, as can be observed in panels b and d of Figure 4, the *m*-methoxy substituents are oriented away from the cluster and the four silver atoms. A close inspection of the extended chain reveals the presence of short C−H···O contacts (d_{HO} = 2.426(13) and 2.755(15) Å; θ_{C-H-O} = 127.24(11)−139.31(11)°)[71−73] between the methoxy oxygen atoms of one $[Pt(2)\{C{\equiv}C(3\text{-}OMe)C_6H_4\}_4]$ unit as acceptors and the C−H protons of the methyl groups (acting as H donors) of the ligands bonded to the fourth platinum (Pt(1#6)) down the chain from that whose substituents act as acceptors. These extended hydrogen bonding contacts engage the external platinum entities of alternate clusters in a way shown in Chart 1, thus contributing to the stability of the chain and probably also to the axial Pt−Pt bond. In fact, each axial Pt−Pt bond is reinforced by two sets of four C−H···O contacts.

Chart 1

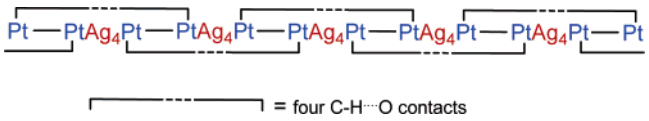

(71) Desiraju, G. R. *Chem. Commun.* **2005**, 2995.
(72) Steiner, T. *Chem. Commun.* **1997**, 727.
(73) Braga, D.; Grepioni, F.; Desiraju, G. R. *J. Organomet. Chem.* **1997**, *548*, 33.

In [**1**]$_\infty$, the Pt···Ag (3.1346(10)−3.1570(11) Å) and Ag···Ag (3.2580(13) and 3.2657(16) Å) distances are rather symmetrical, whereas the Ag···η^2(alkyne) bonds are asymmetrical, with Ag−C$_\alpha$ lengths shorter (Δ 0.171−0.205 Å) than the corresponding Ag−C$_\beta$. The angles at C$_\alpha$, Pt−C$_\alpha$≡C$_\beta$, are nearly linear, whereas those at C$_\beta$ are clearly distorted from 180° (163.2(13)−165.6(18)°).

Photophysical Properties. Absorption and emission data of compounds **1** and **2** together with those of [Pt$_2$Ag$_4$-(C≡CPh)$_8$],[43,50] which has been included for comparative purposes, are summarized in Tables S2 and S3 (see the Supporting Information). Dissolution of garnet form [**1**]$_\infty$ and the related extended, very dark garnet platinum−copper chain derivative **2** (∼5 × 10^{-5} M) leads to a loss of their colors yielding yellow solutions, indicating that their colors came from solid-state effects due to the presence of Pt−Pt bonds. In the solid state, these Pt−Pt bonds in both stacked clusters are observed as a broad absorption centered at 633 nm in [**1**]$_\infty$ and at 680 nm in **2** (see the Supporting Information, Figure S5). This band is assigned as a metal−metal-to-ligand charge transfer (^{3}MMLCT). The remarkable red shift in the platinum−copper derivative is suggestive of a shorter and presumably stronger Pt−Pt bond relative to that found in **1**. This tendency is in agreement with the longer Pt−Pt separation that we have found in the red form of [Pt$_2$Ag$_4$-(C≡CPh)$_8$]$_2$ (3.221(2) Å, see the Supporting Information, Figure S1) with respect to the analogous red form of [Pt$_2$Cu$_4$(C≡CPh)$_8$]$_2$ (3.116(2) Å).[50] Presumably, the stronger η^2-M−alkynyl metal interactions with the copper centers, which are reflected in the lower ν(C≡C) stretching vibrations (2014 cm^{-1}, **2**; 2029 cm^{-1}, [**1**]$_\infty$), play a key role in the final strength of the axial Pt−Pt bond between clusters. The η^2-alkynyl metal d^{10} linkages seem to enhance the Pt−C$_\alpha$ π-acceptor bonding component, which decreases the electron density on platinum. As a consequence, the electronic repulsion between the platinum centers presumably is reduced, favoring the formation of axial Pt−Pt bonds between clusters. The nature of the axial Pt−Pt bond has recently been examined by theoretical calculations (ADF) in the trinuclear compound [Pt(Me$_2$Bpy)$_2$][PtCl$_2$(Me$_2$Bpy)]$_2$[PF$_6$]$_2$, which exhibits a trinuclear Pt−Pt−Pt backbone with a Pt−Pt distance of 3.474(6) Å.[70] This study indicates that the relatively strong Pt−Pt metallic bond (∼40 kcal mol^{-1}) has similar covalent and ionic contributions.[70]

Room-temperature absorption spectra of dilute solutions of **1** and **2** (Figure 5) show high-energy intraligand absorptions and two low-energy spin- and orbital-allowed bands, notably red-shifted in relation to the precursor (NBu$_4$)$_2$[Pt-{C≡C(3-OMe)C$_6$H$_4$}$_4$],[36] which are characteristic of the hexanuclear cluster core [Pt$_2$M$_4${C≡C(3-OMe)C$_6$H$_4$}$_8$]. The lowest absorption occurs at ca. 424 nm in the platinum−copper derivative **2**, being notably blue-shifted in the platinum−silver compound (401 nm). Curiously, this band is unaffected by the solvent in cluster **2**, and is slightly blue-shifted (398 nm) in THF for **1**, presumably reflecting the existence of Ag···O (THF) contacts in this donor solvent, in accordance with the crystal structure of the adduct

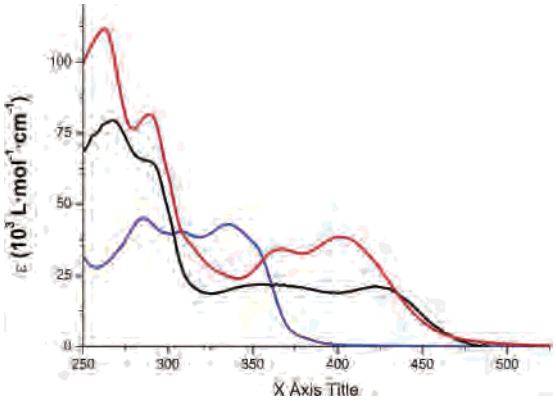

Figure 5. Normalized electronic absorption spectra of (NBu$_4$)$_2$[Pt-{C≡C(3-OMe)C$_6$H$_4$}$_4$] **A** (blue), [Pt$_2$Ag$_4${C≡C(3-OMe)C$_6$H$_4$}$_8$] **1** (red), and [Pt$_2$Cu$_4${C≡C(3-OMe)C$_6$H$_4$}$_8$] **2** (black) in 5 × 10^{-5} M CH$_2$Cl$_2$ at 298 K.

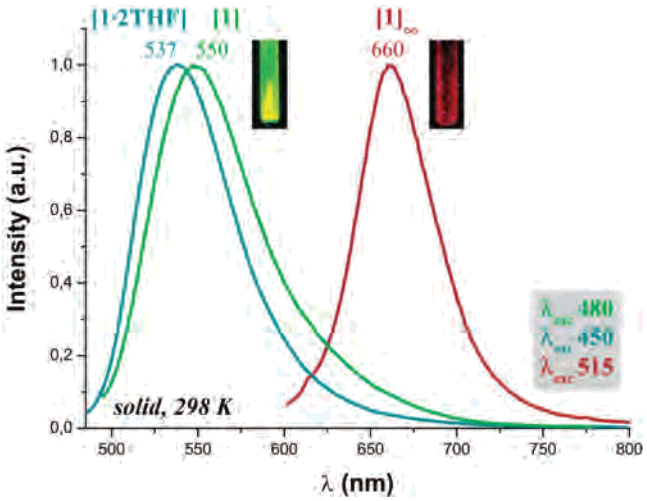

Figure 6. Normalized solid-state (powder) emission spectra of [**1**], [**1·2THF**], and [**1**]$_\infty$ at 298 K.

[**1·2THF**] (Figure 3). Following previous assignments,[45,51,74] we attribute these low-energy absorptions to an admixture of MLCT (Pt/π(C≡CR) → π*(C≡CR)) and LM′CT (ligand or platinum−ligand−M′ charge transfer Pt(C≡CR) → M′(d^{10})) perturbed by Pt···M′ and M′···M′ interactions. Alternatively, the transition may be viewed as a MLM′CT (M = Pt, M′ = d^{10}) mixed with intraligand character.

These clusters are strongly emissive both in solution and in the solid state. The emission spectra of **1**, [**1·2THF**], and [**1**]$_\infty$ in the solid state at room temperature and at 77 K are shown in Figure 6 and the Supporting Information, Figure S6, respectively. As can be observed, the yellow monomer **1** produces an intense green-yellow luminescence centered at 550 nm (λ_{ex} 480 nm, 3.41 μs), which is slightly blue-shifted to 537 nm and visibly less intense in the solid crystalline adduct [**1·2THF**] (λ_{ex} 450 nm, 3.47 μs). These emissions are notably enhanced and slightly red-shifted at 77 K (560 nm, τ 24.3 μs [**1**]; 540 nm, τ 11.2 μs [**1·2THF**]) (see the Supporting Information, Figure S6), but at this temperature, a small low-energy shoulder is also observed

(74) Forniés, J.; Fuertes, S.; Martín, A.; Sicilia, V.; Lalinde, E.; Moreno, M. T. *Chem.—Eur. J.* **2006**, in press.

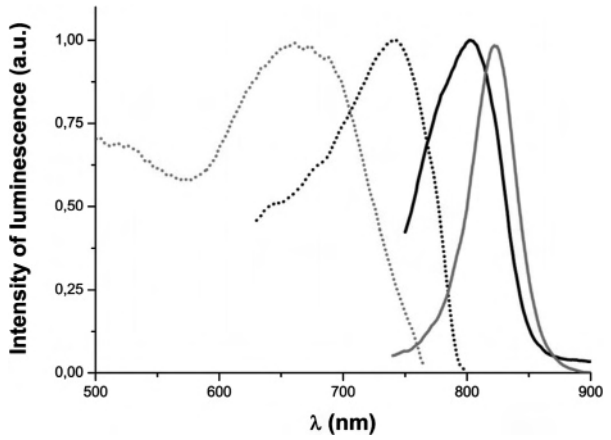

Figure 7. Normalized excitation and emission spectra of $[Pt_2Cu_4\{C{\equiv}C(3\text{-}OMe)C_6H_4\}_8]$ **2** in the solid state (powder): at 298 K, λ_{exc} 630 nm (black solid line) and λ_{em} 815 nm (black dotted line); at 77 K, λ_{exc} 680 nm (grey solid line) and λ_{em} 830 nm (grey dotted line).

(~620 nm, **1**; ~600 nm, [**1.2THF**]). The excitation spectra are similar and resemble the solution absorption spectra, indicating that the emissive states are also characteristic of the hexanuclear cluster core $[Pt_2M_4(C{\equiv}CR)_8]$. They are assigned to emissive states derived from a ^{3}MLM′CT (Pt(d)/π(C≡CR) → Pt(p_z)/Ag(sp)/π*(C≡CR)) state modified by Pt···Ag and Ag···Ag contacts. In accordance with this assignment, these yellow-greenish emissions are very close in energy to those found for the yellow monomer $[Pt_2Ag_4(C{\equiv}CPh)_8]$ (545 nm (298 K), 565 nm (77 K) solid;[50] 570 nm (298 K) KBr pellets[43]). The emissions in these arylethynyl derivatives are considerably red-shifted in relation to that of the previously reported *t*-butylacetylide cluster $[Pt_2Ag_4(C{\equiv}Ct\text{-}Bu)_8]$ (λ_{em} 476 nm),[45] which is consistent with the presence of better π*(C≡C-aryl) accepting orbitals (R = Ph and 3-MeO−C_6H_4).

Crystalline and powdered samples of the garnet form $[\mathbf{1}]_\infty$ show a bright red emission with a λ_{max} of 660 nm and an excited-state lifetime of 0.15 μs (Figure 6). Upon the samples being cooled to 77 K, the emission maximum red-shifts to 707 nm, whereas the excited lifetime increases to 10.1 μs (see the Supporting Information, Figure S6). As can be observed in Figure S6, the excitation spectrum of this emission has a structured excitation profile with peak maxima at 550 and 615 nm, reflecting the solid-state absorption features. This emission is assigned, as in other stacked chain platinum systems, mainly as phosphorescence from a ^{3}MMLCT excited state. According to recent theoretical calculations on Pt···Pt bonding systems,[18,70] the transition presumably involves a platinum-based HOMO corresponding to a dσ* function formed by overlapping d_{z^2} orbitals, which are antibonding with regard to the axial Pt−Pt bond, whereas the LUMO should be located on Pt(p_z) and the ligands (π*C≡CR). In the solid state, the related platinum−copper derivative **2** exhibits (Figure 7) a near-infrared luminescence with an emission maximum at 803 nm and a shoulder at 783 nm, whose Gaussian deconvolution suggests the contribution of two different bands, with maxima at 783 and 815 nm, respectively (see the Supporting Information, Figure S7). At 77 K, the spectral profile narrows considerably (fwhm

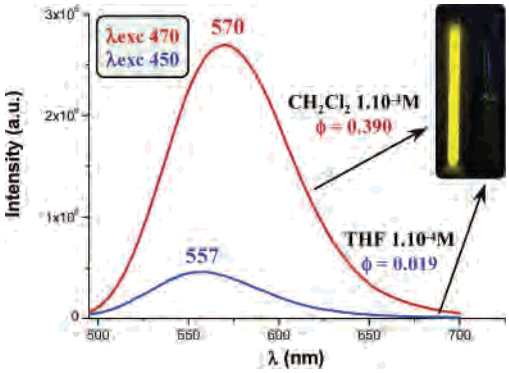

Figure 8. Emission spectra of $[Pt_2Ag_4\{C{\equiv}C(3\text{-}OMe)C_6H_4\}_8]$ **1** in 1 × 10^{-4} M CH_2Cl_2 and 1 × 10^{-4} M THF at 298 K, showing the difference of intensity and quantum yields.

550 cm^{-1}) and shifts to lower energies (λ_{max} 823 nm). The emissions have lifetimes in the microsecond regime. At 77 K, the maximum of the excitation profile shifts to higher energies, giving rise to a larger Stokes shift than at 298 K. This emission resembles that of the trimer derivative $[Pt_2Cu_4(C{\equiv}CPh)_8]_3$ (806 nm), in which the axial Pt···Pt separation is shorter than that found in $[\mathbf{1}]_\infty$ (2.995(1) vs 3.1458(8) Å in $[\mathbf{1}]_\infty$), pointing to the presence of a similar axial Pt···Pt bond in the proposed extended chain structure of **2**. On this basis and assuming a stronger Pt···Pt interaction than that for $[\mathbf{1}]_\infty$, the excited state is likely to have a greater Pt···Pt character. We tentatively propose that the emission originates from an admixture of metal−metal-centered ^{3}(dσ*$p_z\sigma$) and ^{3}MMLCT excited states.

It should be noted that when crystals of the polymeric $[\mathbf{1}]_\infty$ are crushed or exposed to THF vapors, their color and the corresponding emission band does not change. However, by crushing crystals of the yellow solvate [**1·2THF**], we obtain an orange-red powder; the luminescence peaks occur at 560 and 650(max) nm. The color and the low-energy peak are suggestive of the presence of clusters connected by Pt···Pt interactions. For this solvate, [**1·2THF**], the THF molecules are relatively well trapped in the crystal lattice. In fact, the elemental analyses of several old samples are consistent with this formulation, and we have not observed its spontaneous transformation to the red form. The yellow solvate $[Pt_2Ag_4(C{\equiv}CPh)_8]{\cdot}CHCl_3$ shows a similar behavior.

In solution, the luminescence of these clusters depends on the solvent and concentration. Thus, as can be observed in Figure 8, while the platinum silver derivative **1** exhibits in CH_2Cl_2 solution (1 × 10^{-5} to 1 × 10^{-3} M) a bright yellow emission with a very high quantum yield (0.39) centered at 570 nm, in THF solution (10^{-5}−10^{-3} M), the emission is blue-shifted to 557 nm and its intensity drops (Φ = 0.019) so that it is scarcely visible to the naked eye. Both the remarkable quenching and the shift to higher energies are presumably related to the interaction of the silver centers with solvent molecules. It should be mentioned that although the observed emission is essentially nondependent on the concentration, the monitored excitation spectra do depend on it. The emission (570 nm) in a 1 × 10^{-3} M solution is related to an excitation feature centered at 475 nm, whereas monitoring the emission at a lower concentration (1 × 10^{-4}

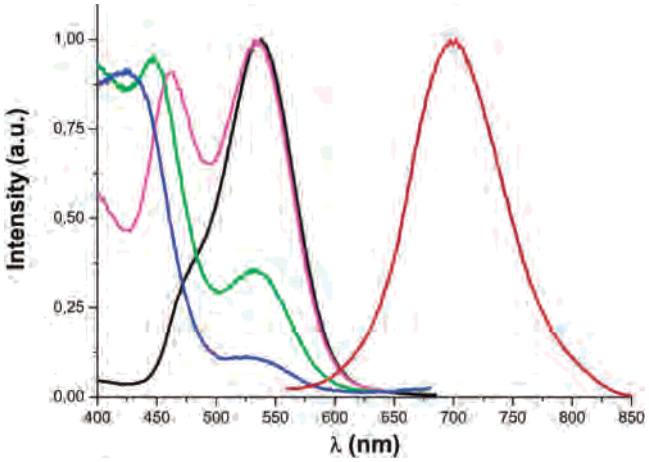

Figure 9. Variation of the excitation spectra of $[Pt_2Cu_4\{C{\equiv}C(3\text{-}OMe)C_6H_4\}_8]$ **2** in $CHCl_3$ (298 K) with the concentration 5×10^{-5} M (blue), 1×10^{-4} M (green), 5×10^{-4} M (red), and 1×10^{-3} M (black) ($\lambda_{em} = 700$ nm in all cases). The emission spectrum (right) is independent of the concentration and the λ_{ex} used.

M) gives rise to an excitation profile with three blue-shifted maxima (344, 373, and 432 nm). Similar behavior is found for $[Pt_2Ag_4(C{\equiv}CPh)_8]$ in fluid solution. In a 1×10^{-4} M CH_2Cl_2 solution, this cluster exhibits a structureless band centered at 570 nm, which is related to several energy excitation peaks (445, 378, and 338 nm). However, the emission in a concentrated solution ($\sim 1 \times 10^{-2}$ M, $\lambda_{em} =$ 566 nm) is related to a low-energy excitation feature at 511 nm. Interestingly, a similar behavior is also observed for the platinum−copper derivative **2**. In fluid $CHCl_3$ solution (298 K), this cluster exhibits a broad emission centered at ca. 700 nm (see Figure 9). As in the platinum−silver derivatives, although the emission is not dependent on the concentration employed in the 5×10^{-5} to 1×10^{-3} M range examined, the excitation spectra change remarkably with the concentration (Figure 9). At low concentration (5×10^{-5} M), the excitation spectrum resembles the absorption spectrum, indicating that the cluster monomer is the absorbing species. As the concentration increases, a new low-energy peak at 535 nm emerges; however, the high-energy feature decreases and shifts slightly, being seen as a shoulder at 480 nm using a concentration of 1×10^{-3} M. The reason for these changes in the excitation spectra are not completely understood but, presumably, could suggest the presence of different absorbing species when the concentration increases. In fact, the solutions do not follow Beer's law at high concentration ($>5 \times 10^{-5}$ M). When the concentration increases, the yellow (**1**) or yellow-orange (**2**) solutions turn orange (**1**) or very dark orange (**2**) and very weak low-energy absorption features at ca. 550 and 600 nm for **1** and **2**, respectively, are discernible. Presumably, cluster monomers Pt_2M_4 are the absorbing species at low concentrations, but as the concentrations increase, the absorbing species are dimers of clusters or higher oligomers, which relax to a similar emissive state following photon absorption. The fluid solution emission of the *m*-methoxyphenylethynyl derivative **1** (CH_2Cl_2, 570 nm) is similar to that of $[Pt_2Ag_4(C{\equiv}CPh)_8]$ (CH_2Cl_2, 570 nm), but it is notably red-shifted in the platinum−copper derivative (700 nm, $CHCl_3$ or CH_2Cl_2), reflecting the contribution of the d^{10} metal centers to the emissive excited state. This tendency (Cu < Ag) has been previously observed in other heteropolynuclear η^2-alkynyl d^{10} complexes; we note that the measured radiative quantum yield (see the Supporting Information, Table S3) decreases by more than 2 orders of magnitude for the platinum−copper cluster in CH_2Cl_2 with respect to the analogous platinum−silver cluster and by more than 1 order in THF solution for both clusters. Following previous work on heteropolynuclear Pt(II) d^{10} alkynyl bridging complexes, we associate the emission with the η^2-coordination Pt−C≡CR → d^{10} and tentatively assign it to a ^{3}MLM′CT (Pt(d)/π(C≡CR) → Pt(p_z)/M′(sp)/π^*) state, strongly modified by Pt···M′ and M′···M′ interactions.

When the sample is cooled to 77 K, the emission in the phenylethynyl platinum−silver derivative $[Pt_2Ag_4(C{\equiv}CPh)_8]$ shifts slightly to lower energy (~575 nm) but the emission does not change with the concentration in the 1×10^{-5} to 1×10^{-3} M range. In contrast to this, the emission spectra of **1** and **2** are significantly altered upon their solutions being cooled. As can be seen in Figure S8 of the Supporting Information, it was found that at a concentration $\geq 1 \times 10^{-3}$ M, the glass of **1** turns red and a new unstructured emission centered at 680 nm develops at the expense of the high-energy emission due to the cluster monomer, which occurs between 570 and 580 nm. This low-energy feature, related to an excitation feature centered at 522 nm, is likely due to the formation of aggregates through axial Pt−Pt bonds and is therefore attributed, as in the solid garnet form $[\mathbf{1}]_\infty$, to phosphorescence from states of a ^{3}MMLCT character. The *m*-methoxyphenylethynyl platinum−copper derivative **2** seems to have a higher tendency to stack; in the range of concentrations examined, between 1×10^{-5} to 1×10^{-3} M, the $CHCl_3$ and CH_2Cl_2 glasses are green (see the Supporting Information, Figure S9). At 77 K, the $CHCl_3$ glass also exhibits two emission maxima at 695 nm and ca. 830−835 nm. The emission at 695 nm resembles that seen at room temperature and has an excitation spectrum with a maximum at 540 nm, whereas the low-energy emission (830−835 nm) has an excitation maximum at 630 nm. The low-energy emission, which is very near to that observed in the solid state (823 nm, 77 K) is also ascribed to aggregate formation via Pt−Pt axial bonds (^{3}MMLCT), whereas the high-energy band (695 nm) is tentatively attributed, as in the fluid room-temperature solution, to emissions derived from a ^{3}MLM′CT emissive state.

Conclusions

In summary, this work shows the remarkable role of the weak noncovalent metal···solvent (Pt···$HCCl_3$ or Ag···O(THF)) and hydrogen (C−H···O) bonding interactions in the structures of the $[Pt_2M_4(C{\equiv}CR)_8]$ clusters. Axial Pt−Pt bonding between clusters is favored for arylethynyl derivatives (R = Ph, (3-OMe)C_6H_4) in nondonor solvents such as CH_2Cl_2 or $CHCl_3$, and is particularly enhanced in the platinum−copper derivatives, presumably by the stronger η^2-alkynyl−Cu bond, as revealed by larger $\Delta\nu$(C≡C) shifts to lower wavenumbers. We propose that the η^2-alkynyl (M = d^{10}) bonding within the clusters enhances the Pt ⇌ C≡R

π acceptor bonding component, decreasing the electron density at the Pt centers. This decrease of the electron density at platinum centers seems to favor the formation of axial Pt−Pt bonds. Thus, whereas $[Pt_2Cu_4(C{\equiv}CPh)_8]$ forms dimers and trimers, the related $[Pt_2Ag_4(C{\equiv}CPh)_8]$ only forms dimers, which coexist with the yellow monomer, exhibiting an extended chain of monomers separated by chloroform molecules due to short Pt···$HCCl_3$ contacts. In the *m*-methoxy derivative $[Pt_2Ag_4\{C{\equiv}C(3\text{-}OMe)C_6H_4\}_8]$, for the garnet form $[\mathbf{1}]_\infty$, the presence of extended C−H···O(OMe) hydrogen bonds between alternate clusters clearly seems to be contributing to the axial Pt···Pt bonding, giving a final 1-D extended network. In the yellow form [**1.2THF**], the solvent molecules interact easily with the silver centers, weakening the η^2-(alkynyl)−Ag. This fact and the cooperative effect of C−H···O contacts between clusters are probably enough to compensate and eliminate the axial Pt−Pt bonds.

The clusters are brightly emissive. The emissions observed for the yellow monomers $[Pt_2Ag_4(C{\equiv}CPh)_8]$, **1**, and [**1·2THF**] in the solid state and in dilute solutions are attributed to a ^{3}MLM′CT (Pt(d)/π(C≡CR) → Pt(p_z)/Ag(sp)/π*(C≡CR)) state, strongly modified by Pt···Ag and Ag···Ag interactions, and in [**1·2THF**] also by Ag···O solvent contacts. The extended forms $[\mathbf{1}]_\infty$ and **2** with strong axial Pt−Pt bonds are less emissive and exhibit phosphorescence, which is tentatively thought to come from an ^{3}MMLCT excited state ($[\mathbf{1}]_\infty$) or an admixture of metal−metal (Pt−Pt)-centered $^3(d\sigma^*p_z\sigma)$ and ^{3}MMLCT excited states. In frozen solution, the tendency to stack increases, as expected, in the platinum−copper derivatives vs the platinum−silver clusters: **2** > **1**; $[Pt_2Cu_4(C{\equiv}CPh)_8]$[43] > $[Pt_2Ag_4(C{\equiv}CPh)_8]$. Substituents also play a role in the tendency to stack. Thus, whereas only one emission (CH_2Cl_2, 77K, 575 nm) due to monomers is observed for $[Pt_2Ag_4(C{\equiv}CPh)_8]$ in the 1×10^{-5} to 1×10^{-3} M range, two emissions at 570−580 nm (monomer) and 680 nm (due to Pt−Pt stacking) are found for $[Pt_2Ag_4\{C{\equiv}C(3\text{-}OMe)\text{-}C_6H_4\}_8]$ **1** at a concentration $\geq 1 \times 10^{-3}$ M.

Acknowledgment. This work was supported by the Spanish Ministerio de Educación y Ciencia (Project CTQ2005-08606-C02-01-02). B.G. thanks the CSIC for a grant.

Supporting Information Available: Tables S1−S3 and Figures S1−S9. Crystallographic data in CIF format. This material is available free of charge via the Internet at http://pubs.acs.org.

IC0608344